Direct Measurement of Solid-Liquid Interfacial Energy Using a Meniscus

Jingcheng Ma, Ishrat Zarin, and Nenad Miljkovic

Direct Measurement of Solid-Liquid Interfacial Energy Using a Meniscus

Jingcheng Ma[1,2]*†, Ishrat Zarin[1]†, and Nenad Miljkovic[1,3,4,5]*

[1]Department of Mechanical Science and Engineering, University of Illinois, Urbana, IL, USA

[2]Current Address: The James Franck Institute, University of Chicago, Chicago, IL, USA

[3]Materials Research Laboratory, University of Illinois, Urbana, IL, USA

[4]Department of Electrical and Computer Engineering, University of Illinois, Urbana, IL, USA

[5]International Institute for Carbon Neutral Energy Research (WPI-I2CNER), Kyushu University, 744 Motooka, Nishi-ku, Fukuoka 819-0395, Japan

†: These authors contributed equally.

Abstract: Solid-liquid interactions are central to diverse processes. The interaction strength can be described by the solid-liquid interfacial free energy (γ_{sl}), a quantity that is difficult to measure. Here, we present the direct experimental measurement of γ_{sl} for a variety of solid materials, from non-polar polymers to highly wetting metals. By attaching a thin solid film on top of a liquid meniscus, we create a solid-liquid interface. The interface determines the curvature of the meniscus, analysis of which yields γ_{sl} with an uncertainty of less than 10%. Measurement of classically challenging metal-water interfaces reveals $\gamma_{sl} \sim 30$ - 60 mJ/m^2, demonstrating quantitatively that water-metal adhesion is 80% stronger than the cohesion energy of bulk water, and experimentally verifying previous quantum chemical calculations.

Keywords: solid-liquid interface, interfacial free energy, capillary, wettability, hydrogen bonds

The interaction between a solid and liquid is essential to many fields [1-3]. Human wellness benefits from understanding of cellular behavior in complex biofluids [4, 5]. The soil and crops in our environment respond to the absorption of rain and agricultural sprays [6]. In energy systems, the affinity of a solid to the working fluid determines the efficiency of boiling and condensation [7, 8]. Within fuel cells and batteries, the electric double layer made up of water molecules near a metal electrode plays a key role in the electrochemistry [9]. To quantitatively describe these solid-liquid interfaces and interactions, the solid-liquid interfacial free energy (γ_{sl}) is used. This free energy arises from the imbalanced force on the liquid surface molecules that are attracted by the solid atoms on one side, and by the bulk liquid on the other side [10].

Although vital to many processes, the direct and accurate measurements of γ_{sl} remains a challenge. The most widely used approach to determine γ_{sl} is the liquid droplet contact angle technique [11, 12], which was first introduced in the 1960s [13]. When a liquid droplet is in contact with a chemically homogenous and smooth solid surface, it shows partial wetting and forms a spherical liquid cap, enabling the estimation of γ_{sl} from the measured droplet contact angle [13]. Although this method works well for soft and low-surface-energy materials such as polymers, it is not applicable for high-energy surfaces like metals, ceramics, or semiconductors, because the droplet spreads and eliminates the ability to measure a finite contact angle [14].

Here, in contrast with the classical approach of probing a droplet, we instead probe a liquid meniscus to directly measure γ_{sl} of a solid surface. We develop the solid-liquid interface by using the following steps: we first let a vertically suspended plate touch a liquid surface and allow a liquid meniscus to form. We then attach a thin and smooth solid film on this liquid meniscus, thus creating a solid-liquid interface that replaces the original liquid-air interface (Figure 1a and 1b). Herein, we define this meniscus as the multilayer solid-liquid meniscus (SL-meniscus) to help differentiate it from a liquid meniscus which describes a free-liquid surface. The curvature of the SL-meniscus changes when compared to a free water meniscus, which is caused by the solid-liquid interfacial interaction, and which enables the measurement of γ_{sl} from analysis of the meniscus profile (Figure 1c).

The SL-meniscus is similar to the well-studied liquid-air meniscus [15]. The shape of liquid meniscus formed on an adjacent vertical solid wall is determined by the equilibrium between the capillary force and the gravitational force. Immediately beneath the meniscus, the Laplace's pressure is equal to the hydrostatic pressure [15]:

$$\rho g y = \sigma_l \kappa_l = -\sigma_l \frac{\ddot{y}(x)}{\left[1 + \dot{y}(x)^2\right]^{1.5}}, \tag{1}$$

where y is the height of the liquid surface above the level of the liquid bath, x is the distance from the vertical wall, ρ is the liquid density, g is gravitational acceleration, κ_l is the meniscus curvature, and σ_l is liquid-vapor surface tension. The Laplace pressure is only contributed to by the principal curvature in the $x - y$ plane. No curvature exists in the orthogonal $y - z$ plane.

For the SL-meniscus, the Laplace pressure originates from the solid-liquid interface, hence the surface tension term in Equation 1 (σ_l) needs to be replaced by solid-liquid interfacial tension (σ_{sl}). The geometry of the SL-meniscus is, therefore, described by:

$$\rho g y = \sigma_{sl} \kappa_{sl}, \tag{2}$$

where κ_{sl} is the SL-meniscus curvature. Measuring the profile of a SL-meniscus allows us to determine σ_{sl}, and sequentially γ_{sl}. We note that the interfacial tension σ_{sl}, which we directly measure, is not always numerically equal to γ_{sl}. Elastic stretching of the solid film also contributes to σ_{sl}. However, the elastic contribution is negligible in our rationally designed thin films system (< 0.1 mJ/m^2) (see Section S2 of the Supplemental Materials).

It is critical to make the solid films sufficiently thin for the described measurement. This ensures that the bending energy (ε_b) is negligible when compared to the meniscus gravitational potential (ε_g). Otherwise, the elasticity of the solid film may change the shape of the meniscus. For soft materials having elastic moduli $E < 1$ GPa, the bending energy becomes significant ($> 10^{-2}\varepsilon_g$) when the solid film thickness $h > 100$ μm. For metals, the critical solid film thickness is $h \sim 1$ μm. Detailed analyses of ε_b and ε_g are included in Section S5 of the Supplemental Material.
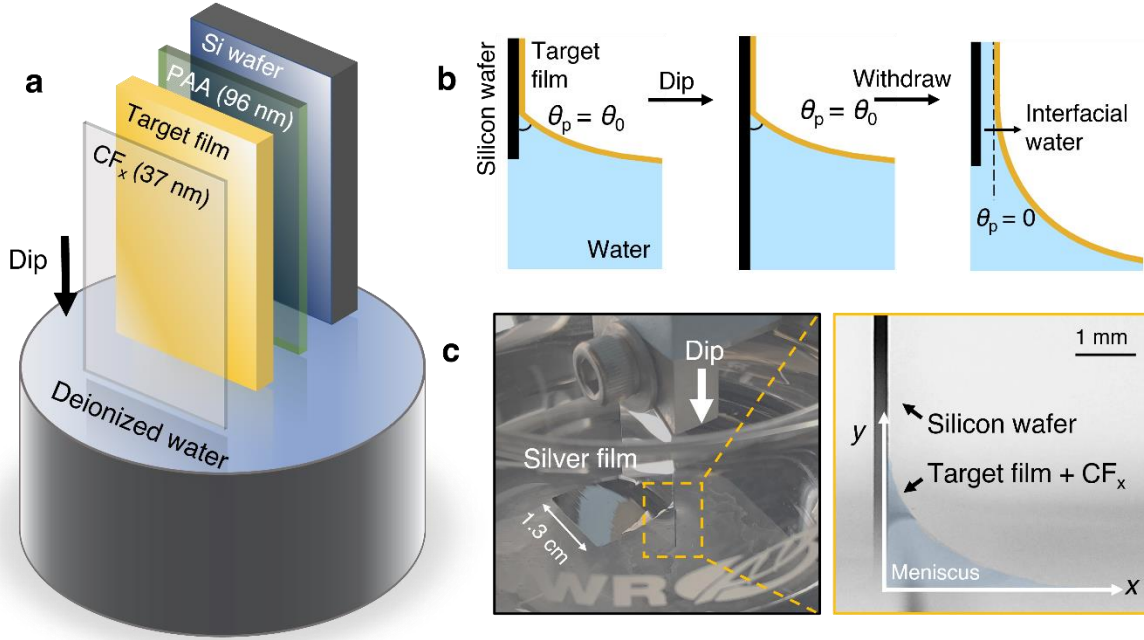
3

Figure 1. Illustration of the measurement procedure. (a) Schematic diagram of the 4-layer sample structure. (b) Schematic diagram of the sample dipping procedure that forms the peeling angle $\theta_p = 0$. (c) Optical images of the experimental setup and the side-view of a silver-water meniscus.

We obtain the SL-meniscus by fabricating a four-layer structured sample (Figure 1a). We used a 2 cm-long, 1.3 cm-wide, and 0.28 mm-thick polished silicon wafer as our substrate. A 96-nm thick, water-soluble polyacrylic acid (PAA) film is first spun-coat on the silicon wafer to act as a sacrificial layer. The target solid film is then deposited on the PAA film. Upon dipping the sample vertically into water, the PAA layer dissolves, and the target film is released and flows on top of the formed liquid meniscus. We found that the PAA film dissolves completely after 30 seconds of water immersion, and the small amount of acrylic acid contamination does not affect the measurement (see Section S5 of the Supplemental Materials). Since the interface is not exposed to the ambient prior to the measurement, we avoid potential contamination from oxidation or volatile organic contamination [16-19]. On the top layer, we deposit a 37 nm-thick fluoropolymer coating to ensure that water flows into the interface to initiate meniscus formation, instead of flowing on top of the sample. Detail of the materials fabrication and characterization are included in Section S1 of the Supplemental Material.

The peeling angle at the peeling front also governs the meniscus cross-sectional profile and affects data collection (θ_p, see Figure 1b) [15, 20, 21]. We experimentally ensure that $\theta_p = 0$ every

time so the meniscus profile solely depends on γ_{sl}. The front angle is determined by $\cos(\theta_p) = 1 - (G_w/\gamma_{sl})$ [20, 21], where G_w is the wet film-substrate adhesion. We first dip the sample into the liquid to a depth of 1.5 cm from the leading edge, then withdraw it by 5 mm, leaving a thin layer (~100 μm-thick, see Supplemental Image S8) of residual liquid in between the film and the substrate (Figure 1b). In this case, the wet adhesion to separate the film and substrate is 0, hence $\cos(\theta_p) = 1$.

The meniscus profile is described by the analytical solution of Eq. (2), expressed as [15]:

$$x_{exp} - \Delta x = l'_c \cosh^{-1}\left(\frac{2l'_c}{y_{exp} + \Delta y}\right) - 2l'_c \sqrt{1 - \frac{(y_{exp} + \Delta y)^2}{4l'^2_c}}, \qquad (3)$$

where $l'_c = \sqrt{\gamma_{sl}/\rho g}$ is the modified capillary-length. The x-axis position parameter (Δx) can be determined using the boundary condition $\theta_p = 0$. A y-axis position parameter (Δy) is introduced because accurately determining $y = 0$ within a ± 0.1 mm uncertainty is difficult due to the blurry liquid surface. Therefore, we defined the vertical position of the lowest data point as $y_{exp} = 0$, and the real vertical position y to be $y = y_{exp} + \Delta y$, where Δy is fitted (typically $\Delta y = 10^{-5}$ to 10^{-4} m). The experimental data set is fitted by the model of Eq. (3) to derive γ_{sl}. The theoretically calculated profiles of SL-menisci for a variety of γ_{sl} are shown in Figure 2. We estimate the uncertainty based on the goodness-of-fit and a 95% confidence interval in the parameter space of γ_{sl} and Δy. All fitting in our experiments have a coefficient of determination $R^2 > 0.99$, with uncertainty of γ_{sl} within 5 to 10%. Accurate determination of Δy can further lower the uncertainty in γ_{sl}.
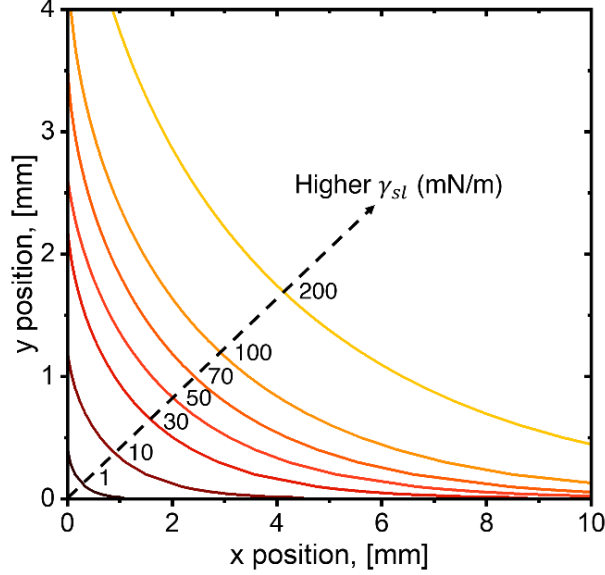
Figure 2. Theoretically calculated (Eq. 3) menisci *x-y* profiles for a variety of γ_{sl} when $\theta_p = 0$.

We benchmark our measurement technique using well-characterized non-polar amorphous polymers, including polystyrene (PS, 199 nm-thick), Teflon-AF (59 nm-thick) and polymethylmethacrylate (PMMA, 170 nm-thick). The non-polar nature of these solids provides convenience to establish reference values of γ_{sl} using classical Fowkes theory, which describes the solid surface free energy (γ_s) as being composed of the dispersive component ($\gamma_{s,d}$) and the polar component ($\gamma_{s,p}$): $\gamma_s = \gamma_{s,d} + \gamma_{s,p}$ [13]. The interfacial free energy is given by [13]:

$$\gamma_{sl} = \gamma_s + \gamma_l - 2\left(\gamma_{s,d}\gamma_{l,d}\right)^{0.5} - 2\left(\gamma_{s,p}\gamma_{l,p}\right)^{0.5}, \tag{4}$$

where the surface energies of solids (γ_s) are measured by contact angle approach [22]. The surface energies of the liquids (γ_l) are obtained from literature. See Section S2 of the Supplemental Material for additional surface energy analysis details.

Measurement on the free water meniscus (without any film) yielded $\gamma_l = 72.9 \pm 5.9$ mJ/m^2, consistent with the surface tension of water at room temperature $\sigma_l \approx 73$ mN/m. For the polymer benchmarks, we did not use the sacrificial layer because capillary peeling can spontaneously occur due to the low polymer-silicon adhesion [20]. Other than water ($\gamma_{l,d} = 21.0$ mJ/m^2, $\gamma_{l,p} = 51.8$ mJ/m^2), we also used ethanol ($\gamma_{l,d} = 18.8$ mJ/m^2, $\gamma_{l,p} = 2.3$ mJ/m^2) to probe low γ_{sl} systems. The

profiles of all seven menisci are shows in Figure 3a, where dashed lines represent lines of best fit. As predicted, the meniscus profile clearly depends on the chemistry of different solid films and testing liquids. A direct comparison between the reference γ_{sl} values and our measurements are included in Figure 3b, demonstrating good agreement. The polymer-ethanol interfaces showed lower γ_{sl} (< 20 mJ/m^2) when compared to polymer-water interfaces, as predicted. However, the measured γ_{sl} for polymer-ethanol interfaces were 5-10 mJ/m^2 higher when compared to Fowkes theory. We hypothesize that charge transfer occurs at the ethanol-polymer interface, similar to past observations at the water-hydrocarbon interface [23], causing ethanol molecule orientation to deviate from its bulk orientation, and sequentially making the liquid hear the surface more polar. Images of all measured menisci are included in Section S3 of the Supplemental Material.
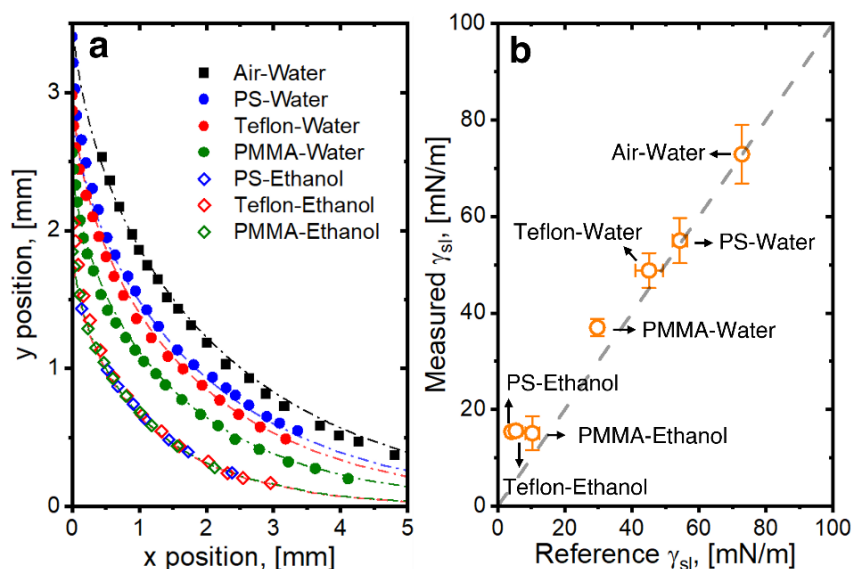

Figure 3. Benchmarking using polymer-liquid interfaces. (a) Comparison between experimental measured (dots) and theoretically calculated (dashed lines) film menisci profiles. Error bars in position are smaller than the symbol size and are not shown. (b) Comparison between the results obtained using the SL-meniscus method (y-axis) and contact angle method (x-axis).

We now demonstrate the capability of our technique to measure highly wetting and rigid materials. We measure γ_{sl} between water and five sputtered metallic films, including inert metal films: gold (180 ± 3 nm thick), silver (176 ± 4 nm thick), platinum (206 ± 3 nm thick), and non-inert metals including aluminum (172 ± 6 nm thick) and titanium (161 ± 6 nm thick). The measured

profiles are included in Figure 4a. The metals were deposited on the PAA surfaces by magnetron sputtering (see Section S1 of the Supplemental Material). The mechanical bending of the metal films having thickness of $\sim$100 nm is not expected to affect the accuracy of the γ_{sl} measurement. Figure 4b shows the bending energy (ε_b) of all films used. When compared to the gravitational potential energy (red solid line), ε_b are all negligible ($<10^{-3}\varepsilon_g$). We also did not observe possible measurement deviations from inclusion of the PAA layer (see Section S4 of the Supplemental Materials).
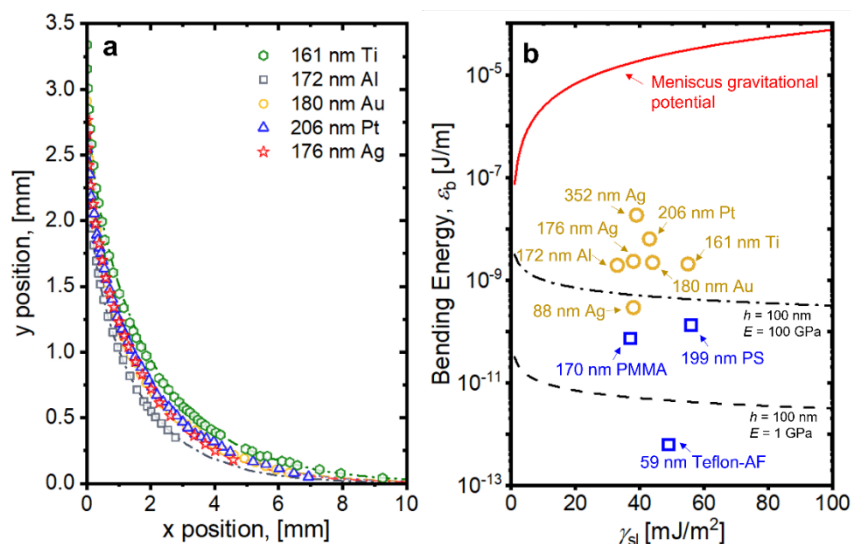

Figure 4. Measurements on water-metal interfaces. (a) Comparison between experiment (data points) and best fit (dashed lines) of the film meniscus profiles. (b) Thin film bending energy (ε_b) as a function of γ_{sl}. Data points represent samples used in our experiments, and the black dashed lines are theoretical values for 100 nm-thick polymer (E = 1GPa) and metal (E = 100GPa) films. The meniscus gravitational potential (ε_g, red solid line) is also included for comparison.

The measured γ_{sl} of all metal-water interfaces ranged from 30 to 60 mJ/m^2. Unexpectedly, they are comparable to the measurement results of the polymer-water interfaces ($\sim$ 50 mJ/m^2), even though the metal surfaces should interact differently with water. We interpret this result as arising from the imbalanced molecular forces between the interfacial water and its bulk. Despite the interfacial water adhering poorly with non-polar polymers and binding strongly with clean metals [2, 24], the interfacial molecular forces are comparably imbalanced with respect to the bulk water hydrogen bonds, resulting in similar γ_{sl} values. The minimum γ_{sl} value is 0 and can be found in between polymers and metals when the solid polarity is water-like, where the molecular

8

forces are perfectly balanced. Therefore, we infer that γ_{sl} for most solids and water is lower than 70 mJ/m^2.

Our measurements provide useful insights into the metal-water interface. Here, we provide two brief discussions on the metal surface energy and mesoscopic wettability, as well as the estimation of the strength of the metal-water hydrogen bond. The mesoscopic wettability of metals, which closely relates to the surface energy of a metal, has been a topic of controversy in the past [12, 13, 25, 26]. Due to complete wetting of water on metals, the exact magnitude of surface energy of a metal γ_s cannot be obtained from the contact angle measurement. Some estimate it to be almost zero [25, 26] while others claim it to be $\sim 10^3$ mJ/m^2 [27]. Here, we obtain the apparent γ_s at water interface using our measured γ_{sl} in combination with Equation 4.

For all metals studied here, $\gamma_{s,d} \approx 50$ mJ/m^2 as measured using the contact angle approach with a non-polar probe fluid diiodomethane (see Sections S2 of the Supplemental Material). Sequentially, the polar surface energy $\gamma_{s,p}$ of our metals can be obtained, which ranged from 150 to 200 mJ/m^2 (see Table 1). This result indicates that metals are highly polar when compared to ceramics and polymers. The measured $\gamma_{s,p}$ values for metals are consistent with conventional wisdom that clean metals are intrinsically hydrophilic from analysis of the Young–Dupre equation: $\cos \alpha = (\gamma_s - \gamma_{sl})/\gamma_l > 1$, where α is the water droplet apparent contact angle. This result ($\cos \alpha > 1$) indicates that the droplet fully spreads on the solid, hence the Young-Dupre equation fails to describe the shape of the droplet. Based on this result, we note that previous works describing clean metals as non-polar owing to delocalization of electrons may not be correct [13, 26]. See Section S7 of the Supplemental Material for additional discussion and comparison with past literature. We also note that recent simulations have revealed that clean metals can appear to be hydrophobic due to the presence of a surface water bilayer closely bonded with the metal surface, leaving no active hydrogen bonds with bulk water [25]. Although the γ_{sl} we measure can indeed be interpreted in this way (see Section S7 of the Supplemental Material), such hydrophobicity is expected of surfaces having well-controlled chemistry and crystal orientation and is unlikely to occur on our sputtered metal surfaces. Examining such effects requires careful control of the surface down to the atomic level.

Our measurements of γ_{sl} also provide insights on the strength of water-metal adhesion, which is mainly governed by metal-water hydrogen bonds. We calculated the water-metal adhesion (G_{sl}) using classical thermodynamics $G_{sl} = \gamma_s + \gamma_l - \gamma_{sl}$ [12, 13], which yielded

9

G_{sl} = 240 to 270 mJ/m^2 at the metal-water interface (see Table 1). This is consistent with simulations based on density functional theory (170 to 240 mJ/m^2) [28]. This value is approximately 80% higher than the cohesion energy of water ($2\gamma_l \approx 140$ mJ/m^2) and 5 to 10 times higher than the polymer-water adhesion. Such high adhesion is expected from the strong water-metal hydrogen bonds between an ice-like interfacial water bilayer on clean metals, as observed by ultra-high vacuum experiments [1, 2, 24].

Table 1. Measured values of γ_{sl}, $\gamma_{s,p}$ and G_{sl} at the polymer-water and metal-water interfaces. Uncertainties of $\gamma_{s,p}$ and G_{sl} were computed using propagation of error.

Solid Material	Solid-water interfacial free energy, γ_{sl} (mJ/m^2)	Solid polar surface energy, $\gamma_{s,p}$ (mJ/m^2)	Solid-water adhesion G_{sl} (mJ/m^2)
Teflon-AF	48.8 ± 3.6	0.1 ± 0.1	33.2 ± 1.7
PS	56.0 ± 4.6	0.0 ± 0.7	59.0 ± 4.7
PMMA	37.1 ± 1.8	16.4 ± 3.4	93.8 ± 4.1
Gold	43.5 ± 2.3	176.2 ± 5.0	255.8 ± 5.6
Silver	38.2 ± 3.1	164.5 ± 7.0	249.4 ± 7.7
Platinum	42.6 ± 1.4	174.7 ± 3.0	254.7 ± 3.3
Aluminum	32.5 ± 1.4	152.6 ± 3.3	241.6 ± 3.6
Titanium	56.2 ± 1.6	202.9 ± 3.2	269.4 ± 3.6

In addition to metals, our technique presented here can provide important benchmark measurements to understand a variety of solid-liquid interfaces, especially for stiff materials such as high-energy inorganic crystals where contact angle methods are not applicable. One limitation of our technique is the lack of general strategies to create the SL-meniscus. Methods which can be applied to any material/working fluid system need further development. Capillary peeling works for a limited amount of interfaces [20], hence developing sacrificial layers for different probe liquids requires future investigation. Currently, the approach used to understand highly-wetting solid-liquid interfaces relies on computational tools, including molecular dynamics (MD) simulations [29, 30], density functional theory (DFT) [1, 3, 31, 32], and machine-learning models [17, 33]. Direct experimental measurement of γ_{sl} provides valuable experimental datasets to optimize these computational tools, demonstrating a promising method to understand solid-liquid interfaces, and to enable reliable closed-loop design of materials and surfaces for numerous applications.

Associated Content

Supplemental Material

S1. Materials fabrication and characterization.

S2. Deviation between σ_{sl} and γ_{sl}.

S3. Measurement of γ_{sl} using the contact angle method.

S4. Raw images of all measured menisci.

S5. Dissolving the PAA film.

S6. Energy comparison between thin film bending and meniscus gravitational potential.

S7. Supplemental discussion about the wettability of metals.

S8. Formation of a residual water layer after sample retraction.

The Supplemental Material also includes the following Supplemental References: [1-3, 13, 16, 18, 20, 24-26, 34-51]

Author Information

Corresponding Authors

*Jingcheng Ma: jcma36@illinois.edu

  Current email address: jcma36@uchicago.edu

*Nenad Miljkovic: nmiljkov@illinois.edu

Notes

Conflict of interest: The authors declare no competing financial interests.

References

1.   Carrasco, J., A. Hodgson, and A. Michaelides, *A molecular perspective of water at metal interfaces.* Nature Materials, 2012. **11**(8): p. 667-674.
2.   Thiel, P.A. and T.E. Madey, *The Interaction of Water with Solid-Surfaces - Fundamental-Aspects.* Surface Science Reports, 1987. **7**(6-8): p. 211-385.
3.   Bjornehohn, E., M.H. Hansen, A. Hodgson, L.M. Liu, D.T. Limmer, A. Michaelides, P. Pedevilla, J. Rossmeisl, H. Shen, G. Tocci, E. Tyrode, M.M. Walz, J. Werner, and H. Bluhm, *Water at Interfaces.* Chemical Reviews, 2016. **116**(13): p. 7698-7726.
4.   Weirich, K.L., S. Banerjee, K. Dasbiswas, T.A. Witten, S. Vaikuntanathan, and M.L. Gardel, *Liquid behavior of cross- linked actin bundles.* Proceedings of the National Academy of Sciences of the United States of America, 2017. **114**(9): p. 2131-2136.
5.   Jiang, Y.W. and B.Z. Tian, *Inorganic semiconductor biointerfaces.* Nature Reviews Materials, 2018. **3**(12): p. 473-490.
6.   Damak, M., S.R. Mahmoudi, M.N. Hyder, and K.K. Varanasi, *Enhancing droplet deposition through in-situ precipitation.* Nature Communications, 2016. **7**: p. 1-9.
7.   Boreyko, J.B. and C.H. Chen, *Self-Propelled Dropwise Condensate on Superhydrophobic Surfaces.* Physical Review Letters, 2009. **103**(18).
8.   Miljkovic, N., R. Enright, and E.N. Wang, *Effect of Droplet Morphology on Growth Dynamics and Heat Transfer during Condensation on Superhydrophobic Nanostructured Surfaces.* ACS Nano, 2012. **6**(2): p. 1776-1785.
9.   Benaglia, S., M.R. Uhlig, J. Hernandez-Munoz, E. Chacon, P. Tarazona, and R. Garcia, *Tip Charge Dependence of Three-Dimensional AFM Mapping of Concentrated Ionic Solutions.* Physical Review Letters, 2021. **127**(19).
10.   Berry, T., *Encyclopedia of physical science and technology, 3rd edition.* Library Journal, 2002. **127**(9): p. 82-+.
11.   Cha, H., J. Ma, Y.S. Kim, L.N. Li, L.W. Sun, J.S. Tong, and N. Miljkoyic, *In Situ Droplet Microgoniometry Using Optical Microscopy.* ACS Nano, 2019. **13**(11): p. 13343-13353.
12.   Fowkes, F.M., *Additivity of Intermolecular Forces at Interfaces .1. Determination of Contribution to Surface and Interfacial Tensions of Dispersion Forces in Various Liquids.* Journal of Physical Chemistry, 1963. **67**(12): p. 2538-&.
13.   Fowkes, F.M., *Attractive Forces at Interfaces.* Industrial and Engineering Chemistry, 1964. **56**(12): p. 40-&.
14.   Quere, D., *Wetting and roughness.* Annual Review of Materials Research, 2008. **38**: p. 71-99.
15.   De Gennes, P.-G., F. Brochard-Wyart, and D. Quéré, *Capillarity and wetting phenomena: drops, bubbles, pearls, waves.* 2013, New York, NY: Springer Science & Business Media. p. 43-47.
16.   Yan, X., Z.Y. Huang, S. Sett, J. Oh, H. Cha, L.N. Li, L.Z. Feng, Y.F. Wu, C.Y. Zhao, D. Orejon, F. Chen, and N. Miljkovic, *Atmosphere-Mediated Superhydrophobicity of Rationally Designed Micro/Nanostructured Surfaces.* Acs Nano, 2019. **13**(4): p. 4160-4173.
17.   Freitas, R. and E.J. Reed, *Uncovering the effects of interface-induced ordering of liquid on crystal growth using machine learning.* Nature Communications, 2020. **11**(1).

18. Li, J., Y. Zhao, J. Ma, W. Fu, X. Yan, K.F. Rabbi, and N. Miljkovic, *Superior Antidegeneration Hierarchical Nanoengineered Wicking Surfaces for Boiling Enhancement.* Advanced Functional Materials, 2021. **n/a**(n/a): p. 2108836.

19. Preston, D.J., N. Miljkovic, J. Sack, R. Enright, J. Queeney, and E.N. Wang, *Effect of hydrocarbon adsorption on the wettability of rare earth oxide ceramics.* Applied Physics Letters, 2014. **105**(1).

20. Ma, J., J.M. Kim, M.J. Hoque, K.J. Thompson, S. Nam, D.C. Cahill, and N. Miljkovic, *Role of Thin Film Adhesion on Capillary Peeling.* Nano Letters, 2021. **1c03494**.

21. Khodaparast, S., F. Boulogne, C. Poulard, and H.A. Stone, *Water-Based Peeling of Thin Hydrophobic Films.* Physical Review Letters, 2017. **119**(15).

22. Ma, J.C., D.G. Cahill, and N. Miljkovic, *Condensation Induced Blistering as a Measurement Technique for the Adhesion Energy of Nanoscale Polymer Films.* Nano Letters, 2020. **20**(5): p. 3918-3924.

23. Pullanchery, S., S. Kulik, B. Rehl, A. Hassanali, and S. Roke, *Charge transfer across C-H center dot center dot center dot O hydrogen bonds stabilizes oil droplets in water.* Science, 2021. **374**(6573): p. 1366-+.

24. Ogasawara, H., B. Brena, D. Nordlund, M. Nyberg, A. Pelmenschikov, L.G.M. Pettersson, and A. Nilsson, *Structure and bonding of water on Pt(111).* Physical Review Letters, 2002. **89**(27).

25. Limmer, D.T., A.P. Willard, P. Madden, and D. Chandler, *Hydration of metal surfaces can be dynamically heterogeneous and hydrophobic.* Proceedings of the National Academy of Sciences of the United States of America, 2013. **110**(11): p. 4200-4205.

26. Schrader, M.E., *Wettability of Clean Metal-Surfaces.* Journal of Colloid and Interface Science, 1984. **100**(2): p. 372-380.

27. Vitos, L., A.V. Ruban, H.L. Skriver, and J. Kollar, *The surface energy of metals.* Surface Science, 1998. **411**(1-2): p. 186-202.

28. Gim, S., K.J. Cho, H.K. Lim, and H. Kim, *Structure, Dynamics, and Wettability of Water at Metal Interfaces.* Scientific Reports, 2019. **9**.

29. Yin, T.Y., D. Shin, J. Frechette, C.E. Colosqui, and G. Drazer, *Dynamic Effects on the Mobilization of a Deposited Nanoparticle by a Moving Liquid-Liquid Interface.* Physical Review Letters, 2018. **121**(23).

30. Srinivas, G., S.O. Nielsen, P.B. Moore, and M.L. Klein, *Molecular dynamics simulations of surfactant self-organization at a solid-liquid interface.* Journal of the American Chemical Society, 2006. **128**(3): p. 848-853.

31. Curtin, W.A., *Density-Functional Theory of the Solid-Liquid Interface.* Physical Review Letters, 1987. **59**(11): p. 1228-1231.

32. Lu, J.Y., Q.Y. Ge, H.X. Li, A. Raza, and T.J. Zhang, *Direct Prediction of Calcite Surface Wettability with First-Principles Quantum Simulation.* Journal of Physical Chemistry Letters, 2017. **8**(21): p. 5309-5316.

33. Schran, C., F.L. Thiemann, P. Rowe, E.A. Muller, O. Marsalek, and A. Michaelides, *Machine learning potentials for complex aqueous made.* Proceedings of the National Academy of Sciences of the United States of America, 2021. **118**(38).

34. See Supplemental Material [url] for additonal details, analysis, and discussions, which includes Refs. [35-51]:

35. Xie, X., K.X. Yang, D.Y. Li, T.H. Tsai, J. Shin, P.V. Braun, and D.G. Cahill, *High and low thermal conductivity of amorphous macromolecules.* Physical Review B, 2017. **95**(3).

36. Grunewal.H, *Weast,Rc - Crc Handbook of Chemistry and Physics.* Angewandte Chemie-International Edition, 1966. **5**(10): p. 907-+.

37. Xu, Q., K.E. Jensen, R. Boltyanskiy, R. Sarfati, R.W. Style, and E.R. Dufresne, *Direct measurement of strain-dependent solid surface stress.* Nature Communications, 2017. **8**.

38. Shuttleworth, R., *The Surface Tension of Solids.* Proceedings of the Physical Society of London Section A, 1950. **63**(365): p. 444-457.

39. Orowan, E., *Surface Energy and Surface Tension in Solids and Liquids.* Proceedings of the Royal Society of London Series a-Mathematical and Physical Sciences, 1970. **316**(1527): p. 473-&.

40. Mondal, S., M. Phukan, and A. Ghatak, *Estimation of solid–liquid interfacial tension using curved surface of a soft solid.* Proceedings of the National Academy of Sciences, 2015. **112**(41): p. 12563.

41. Schulman, R.D., M. Trejo, T. Salez, E. Raphael, and K. Dalnoki-Veress, *Surface energy of strained amorphous solids.* Nature Communications, 2018. **9**.

42. Fowkes, F.M., *Additivity of Intermolecular Forces at Interfaces. I. Determination of the Contribution to Surface and Interfacial Tensions of Dispersion Forces in Various Liquids.* The Journal of Physical Chemistry, 1963. **67**(12): p. 2538-2541.

43. Cha, H., J. Ma, Y.S. Kim, L. Li, L. Sun, J. Tong, and N. Miljkovic, *In Situ Droplet Microgoniometry Using Optical Microscopy.* ACS Nano, 2019. **13**(11): p. 13343-13353.

44. Zhang, Y., M.T. Yin, Y. Baek, K. Lee, G. Zangari, L.H. Cai, and B.X. Xu, *Capillary transfer of soft films.* Proceedings of the National Academy of Sciences of the United States of America, 2020. **117**(10): p. 5210-5216.

45. Rafiee, J., X. Mi, H. Gullapalli, A.V. Thomas, F. Yavari, Y.F. Shi, P.M. Ajayan, and N.A. Koratkar, *Wetting transparency of graphene.* Nature Materials, 2012. **11**(3): p. 217-222.

46. Lifshitz, E.M., *The Theory of Molecular Attractive Forces between Solids.* Soviet Physics Jetp-Ussr, 1956. **2**(1): p. 73-83.

47. Van Oss, C.J., M.K. Chaudhury, and R.J. Good, *Interfacial Lifshitz-van der Waals and polar interactions in macroscopic systems.* Chemical Reviews, 1988. **88**(6): p. 927-941.

48. Tolias, P., *Non-retarded room temperature Hamaker constants between elemental metals.* Surface Science, 2020. **700**.

49. Feibelman, P.J., G.A. Kimmel, R.S. Smith, N.G. Petrik, T. Zubkov, and B.D. Kay, *A unique vibrational signature of rotated water monolayers on Pt(111): Predicted and observed.* Journal of Chemical Physics, 2011. **134**(20).

50. Shih, C.J., Q.H. Wang, S.C. Lin, K.C. Park, Z. Jin, M.S. Strano, and D. Blankschtein, *Breakdown in the Wetting Transparency of Graphene (vol 109, 176101, 2012).* Physical Review Letters, 2015. **115**(4).

51. Lu, H.M. and Q. Jiang, *Surface tension and its temperature coefficient for liquid metals.* Journal of Physical Chemistry B, 2005. **109**(32): p. 15463-15468.